Received: 15 April 2025 | Revised: 22 July 2025 | Accepted: 13 September 2025

DOI: 10.1002/suco.70336

ARTICLE

fib CEB-FIP WILEY

Impact of half-joint failures on RC girder bridges: A robustness quantification study

Paolo Martinelli | **Matteo Colombo**

Department of Civil and Environmental Engineering, Politecnico di Milano, Milan, Italy

Correspondence
Paolo Martinelli, Department of Civil and Environmental Engineering, Politecnico di Milano, Piazza Leonardo da Vinci 32, 20133 Milan, Italy.
Email: paolo.martinelli@polimi.it

Abstract

The robustness of bridge structures is critical to ensuring safety and service continuity, particularly in aging infrastructure exposed to degradation and unexpected loads. Reinforced concrete (RC) half-joint bridges—widely built in Italy between the 1950s and 1970s—exhibit specific vulnerabilities due to inspection challenges, durability concerns, and susceptibility to progressive collapse. Although increasingly studied, the literature lacks comprehensive robustness assessments accounting for full nonlinear system behavior under local damage. This study addresses this gap by developing a refined finite element (FE) modeling approach to simulate the global response of RC half-joint bridges following localized damage. The model includes material nonlinearities throughout the structure and evaluates robustness indicators using a notional removal strategy. The methodology is applied to the Annone viaduct, which collapsed in 2016 in northern Italy. The case study serves to analyse failure mechanisms linked to Gerber saddles. Results demonstrate the effectiveness of robustness indicators in capturing force redistribution and progressive collapse in half-joint bridges. The study offers insights into beam–slab interaction and shows how numerical models can support risk-based maintenance and decision-making. The proposed framework enhances assessment strategies for structurally critical bridges and supports future monitoring and mitigation guidelines.

KEYWORDS

accidental actions, beam bridge, half-joint, numerical modeling, progressive collapse, structural robustness

1 | INTRODUCTION

The robustness of bridge structures is a fundamental aspect of transportation infrastructure resilience, directly influencing safety, durability, and overall network reliability. As aging bridges face increasing challenges due to environmental degradation, growing traffic loads, and unforeseen extreme events, the need for systematic and quantitative methods to assess structural robustness has become more pressing. Despite the extensive research conducted on robustness assessment in building structures, its application to bridges remains relatively underdeveloped. A review of disproportionate collapse typologies for various bridge

systems can be found in Starossek[1] and Derseh and Mohammed.[2]

Existing studies on bridge robustness encompass both qualitative and quantitative assessments, often supported by case studies,[3–20] while strategies aimed at enhancing robustness have been explored in prior works.[13,21] Methodologies for quantifying robustness are generally divided into deterministic and probabilistic approaches, as summarized in the JRC technical report.[22]

From a deterministic perspective, several studies have analyzed bridge robustness under different conditions. Wisniewski et al.[3] investigated a four-span continuous reinforced concrete (RC) bridge, while Cavaco et al.[9] examined the impact of corrosion on two RC footbridges. Moreira et al.[23] focused on a masonry arch railway bridge, and Caredda et al.[18] assessed the robustness of a steel truss bridge by simulating various damage scenarios, including non-simultaneous structural element failures. Probabilistic approaches have also been explored: Biondini and Frangopol[24] analyzed the life-cycle robustness of an RC bridge pier with a box cross-section, whereas Björnsson and Thelandersson[25] investigated the structural robustness of a multi-span post-tensioned RC bridge subjected to train collision scenarios.

Over the past decade, several bridge collapses in Italy have underscored the urgent need for reliable robustness assessment methodologies, which can serve as valuable tools for infrastructure authorities in prioritizing maintenance and intervention strategies. Within this framework, significant attention has been directed toward half-joint bridges, a typology that has become particularly relevant due to its structural vulnerabilities.

Half-joints, also referred to as Gerber joints, represent a structural solution widely adopted in Italy between the 1950s and 1970s. This design, introduced by German engineer Heinrich Gerber (1832–1912), facilitates beam construction with reduced-depth ends supported by corresponding cantilevering elements, creating an internal hinge in concrete girders while maintaining a continuous deck surface. A statistical analysis on the construction typologies of prestressed reinforced concrete bridges in Italy[26] revealed that Gerber joints were present in 12% of bridges built in the 1950s and 9.3% of those constructed in the 1970s. However, their use significantly declined in the 1960s, likely due to the increasing adoption of pretensioned prestressing techniques. Furthermore, an internal report by Autostrade per l'Italia (ASPI) in 2022[27] identified that approximately 5% of the 1954 bridges with spans exceeding 10 meters in their network feature reinforced concrete half-joints.

Despite their initial advantages in construction efficiency, half-joint bridges are no longer favored in Italy due to recurring durability issues, primarily related to water leakage, concrete deterioration, and reinforcement corrosion. Originally designed for railway applications—where water accumulation was not a critical concern—the L-shaped geometry of half-joints presents significant challenges for inspection and maintenance. The inaccessibility of internal components complicates the early detection of deterioration, increasing the risk of structural damage. As many of these bridges approach the end of their service life, these concerns become increasingly critical, necessitating focused research and improved maintenance strategies. Recognizing these vulnerabilities, the Italian Guidelines for the Classification, Assessment, and Management of Bridges[28] classify half-joints as "critical elements," highlighting their susceptibility to degradation and their potential to significantly impact overall bridge performance.

To address these concerns, extensive research has been conducted to better understand the structural behavior of half-joints through both experimental and numerical investigations. Laboratory testing has provided valuable insights into the influence of reinforcement detailing on performance, as documented in several studies.[29–33] Concurrently, nonlinear finite element (FE) modeling has emerged as a powerful tool for analyzing half-joints, both in controlled laboratory environments[34] and in existing bridge structures.[35,36] A significant contribution by Flores Ferreira et al.[37] established a benchmark study assessing the reliability of FE models in predicting the structural response of reinforced concrete half-joint beams, comparing numerical simulations with experimental data. However, a comprehensive evaluation of global bridge robustness under half-joint failure remains limited.

Building upon prior work by Martinelli et al.,[38] this study aims to address a specific gap in the existing literature: the limited application of comprehensive nonlinear modeling techniques for assessing the robustness of half-joint RC bridges under local failure scenarios. While previous studies have primarily focused on the localized nonlinearity of Gerber joints or employed simplified linear models, there is a lack of in-depth analyses that consider the full nonlinear behavior of the entire structural system.

To bridge this gap, the present research develops a refined numerical modeling approach that captures the global response of a half-joint bridge to local damage. This methodology extends beyond prior models by incorporating material nonlinearities across all structural components—not just at the half-joint—thereby enabling a more accurate and realistic assessment of load redistribution mechanisms and progressive collapse potential. As a case study, the Annone viaduct is analyzed—an RC half-joint bridge constructed in the 1960s in northern

Italy, which catastrophically collapsed in 2016 under the weight of a heavy truck, resulting in a fatal incident. Investigations by di Prisco et al.[39] revealed pre-existing damage, material degradation, overloading, and design deficiencies in the half-joints. This tragic event exemplifies the need for improved robustness assessments and more effective maintenance protocols to mitigate similar failures in aging bridge infrastructure.

The novelty of this work lies in the application of deterministic robustness indicators, originally developed for simple truss systems, to RC half-joint bridges, and in demonstrating their effectiveness through a notional removal approach tailored to this specific typology. In doing so, the study provides new insights into the role of Gerber saddles and beam-slab interaction in sustaining structural integrity after local damage. The significance of this research is twofold: it enhances the understanding of robustness in a structurally vulnerable class of bridges, and it contributes to the development of more reliable assessment frameworks that can inform maintenance prioritization and risk mitigation strategies.

This paper is structured as follows: Section 2 introduces key robustness indicators from the existing literature, which are later employed in the analysis. Section 3 provides an overview of the case study bridge, detailing its main geometric characteristics and the assumed load configuration. Section 4 outlines a notional removal approach for evaluating the structural robustness of half-joint bridges. Section 5 describes the development of nonlinear finite element models. The results are analyzed and critically discussed in Section 6. Finally, Section 7 summarizes the main conclusions and offers practical recommendations.

2 | STRUCTURAL ROBUSTNESS INDICATORS

Quantifying the robustness of buildings and bridges is crucial for mitigating the risk of progressive collapse, estimating potential losses, and establishing acceptable safety thresholds. Objective robustness measures enable informed decision-making regarding structural safety and facilitate the prioritization of maintenance and repair efforts for existing structures. Various indicators for robustness assessment, encompassing deterministic, probabilistic, and risk-based formulations, have been proposed in the literature. A comprehensive review of these measures is provided by Adam et al.[40] and André et al.[22] However, no universally accepted metric has been established, posing challenges to the widespread adoption of robustness indicators.

Deterministic methods assess structural performance by comparing key parameters—such as stiffness and strength—between the intact and damaged states. In this study, deterministic indicators are intentionally adopted for their simplicity, ease of implementation, and accessibility to practicing engineers, without requiring advanced expertise in probabilistic or risk-based analysis. Although probability-based and reliability-based indicators offer a more comprehensive framework by accounting for uncertainties, and risk-based approaches can include failure consequences when properly quantified, these methods are inherently more complex and demand input data and specialized knowledge that is not always available in standard design practice. The choice of deterministic indicators thus reflects the objective of providing practical robustness assessment tools that can be readily applied in typical engineering workflows.

To evaluate the robustness of a half-joint bridge, the Annone overpass, under various support removal scenarios, three indices are employed. Two of these, ρ_s and ρ_Φ, were introduced by Biondini and Restelli,[41] while the third, the residual redundancy factor R_3, is based on ultimate bearing capacity following the approach of Frangopol and Curley.[42]

The displacement-based robustness index ρ_s is defined as:

$$\rho_s = \frac{\| \mathbf{s}_0 \|}{\| \mathbf{s}_1 \|} \tag{1}$$

where ρ_s represents the ratio of the Euclidean norm ($\| \bullet \|$) of the displacement vector $\mathbf{s}$ in the intact state (subscript "0") to that in the damaged state (subscript "1"). The energy-based robustness index ρ_Φ is given by:

$$\rho_\Phi = \frac{\Phi_0}{\Phi_1} \tag{2}$$

where Φ denotes the stored energy, capturing the variation between intact and damaged conditions. While initially formulated for linear systems, both ρ_s and ρ_Φ can also be applied to nonlinear systems. Lastly, the index R_3 quantifies robustness in terms of ultimate bearing capacity (L), comparing the damaged and intact states:

$$R_3 = \frac{L_{\text{damaged}}}{L_{\text{intact}}} \tag{3}$$

These robustness indices—ρ_s, ρ_Φ, and R_3—are dependent on the specific loading conditions considered, making them "threat-dependent" indicators. Their application, comparison, and discussion within the context of the case study are presented in the following sections, examining notional removal scenarios.

3 | CASE STUDY: ANNONE VIADUCT

The Annone overpass, a precast concrete bridge constructed in the 1960s, serves as the case study for this research. In 2016, the bridge collapsed due to shear failure at one of its Gerber joints while a heavy truck was crossing. Located in the village of Annone, northern Italy, the bridge featured a central suspended span (or "drop-in") flanked by two cantilever side spans, with a total length of 56.10 m and a width of 7.4 m (Figure 1). The side spans were supported by abutments and intermediate walls, each incorporating a 2.80 m cantilever section. The main beams of the central span were supported by half-joints, with each joint comprising five Gerber saddles. The central beams spanned 19.0 m. A horizontal cross-section of both the central and side spans is shown in Figure 1b. The bridge load-bearing system consisted of five prestressed precast beams (PC beams), spaced at 1.35 m along the transverse axis, supporting a continuous cast-in-situ RC slab (Figure 1c). The RC slab was clamped at the abutments, while RC transversal beams—five in the central span and four in the side spans—were cast in situ, running perpendicular to the bridge's longitudinal axis. For further details on the bridge geometry and reinforcement specifications, see di Prisco et al.[39]

The structure was originally classified as a second-category bridge under Circular No. 384 of 14 February 1962,[43] which distinguished between first- and second-category bridges. First-category bridges permitted the passage of "military loads," requiring higher traffic loads in the design calculations, whereas second-category bridges were intended for lower-ranking roads and designed for lighter traffic loads. Although the structure was designed as a second-category bridge, road operators were unaware of its classification and, as a result, exceptional loads were routinely allowed to cross the bridge.

The nominal loads applied to the central span, including self-weight and a single live load configuration, are detailed as follows. The total self-weight—including safety barriers, pavement, curbs, beams, and the RC slab—amounted to 1690 kN, exceeding the original design assumption of 1521 kN. Figure 2 illustrates load placements and naming conventions for the 10 half-joints (R1–R10). The load configuration represents lane 1 subjected to an 8-axle heavy truck, which triggered the failure of half-joint R1, ultimately causing the collapse. The loads P_E, P_F, and P_G in Figure 2 correspond to concentrated forces exerted by the truck weight, transmitted through its wheels. The total live load for this scenario was 1055.6 kN, nearly twice the original design assumption for a single travel lane. In the following simulations, this load configuration is adopted, with the self-weight held constant while the truck load is scaled using a load multiplier (α) applied uniformly to P_E, P_F, and P_G. A value of $\alpha = 1$ represents the full application of the 1055.6 kN live load.

In a previous study,[38] five different load configurations were analyzed, including those based on the original design code,[43] the current Italian code (NTC 2018),[44] and the heavy truck load that triggered the bridge collapse. Among these, the heavy truck configuration generally resulted in lower robustness indicator values and was applied on a single lane, making it suitable for capturing torsional and transverse bending effects. For these reasons, the heavy truck configuration is adopted in the present study.

4 | NOTIONAL REMOVAL SCENARIOS

The design of structures to withstand unspecified hazards can be addressed using a notional damage scenario approach.[45] This method involves two main strategies: (i) notional deterioration scenarios, in which structural properties are degraded and assessed for disproportionate consequences, and (ii) notional removal scenarios, where structural elements are removed to evaluate their impact, potentially considering an alternative load path design. Key components such as columns, panels/walls, or other critical structural elements can be notionally removed to assess robustness.

Notional removal scenarios, commonly used to evaluate building robustness (e.g., Rodríguez et al.,[46] Martinelli et al.[47]), are applied to the bridge under study by sequentially removing half-joints—specifically, the lower nib of the side-span PC beams. Each scenario involves the removal of one half-joint at a time, as illustrated in Figure 3, with half-joint R3 taken as an example. This approach is more conservative than the notional deterioration scenario, as it eliminates entire structural elements rather than merely reducing stiffness or load-bearing capacity. The half-joint removal procedure adopted here follows the methodology recently proposed by the same authors in reference to a simplified finite element model of the bridge.[38] Since a key objective of this study is to assess the influence of numerical model complexity on robustness evaluation, some previous results will be revisited in Section 6.

Half-joint collapses in bridges can result from various factors, with inadequate maintenance being a primary concern. Poor maintenance can lead to corrosion, rust, and structural deterioration, weakening the joints over time and increasing the risk of failure. Other contributing factors include overloading, design or construction

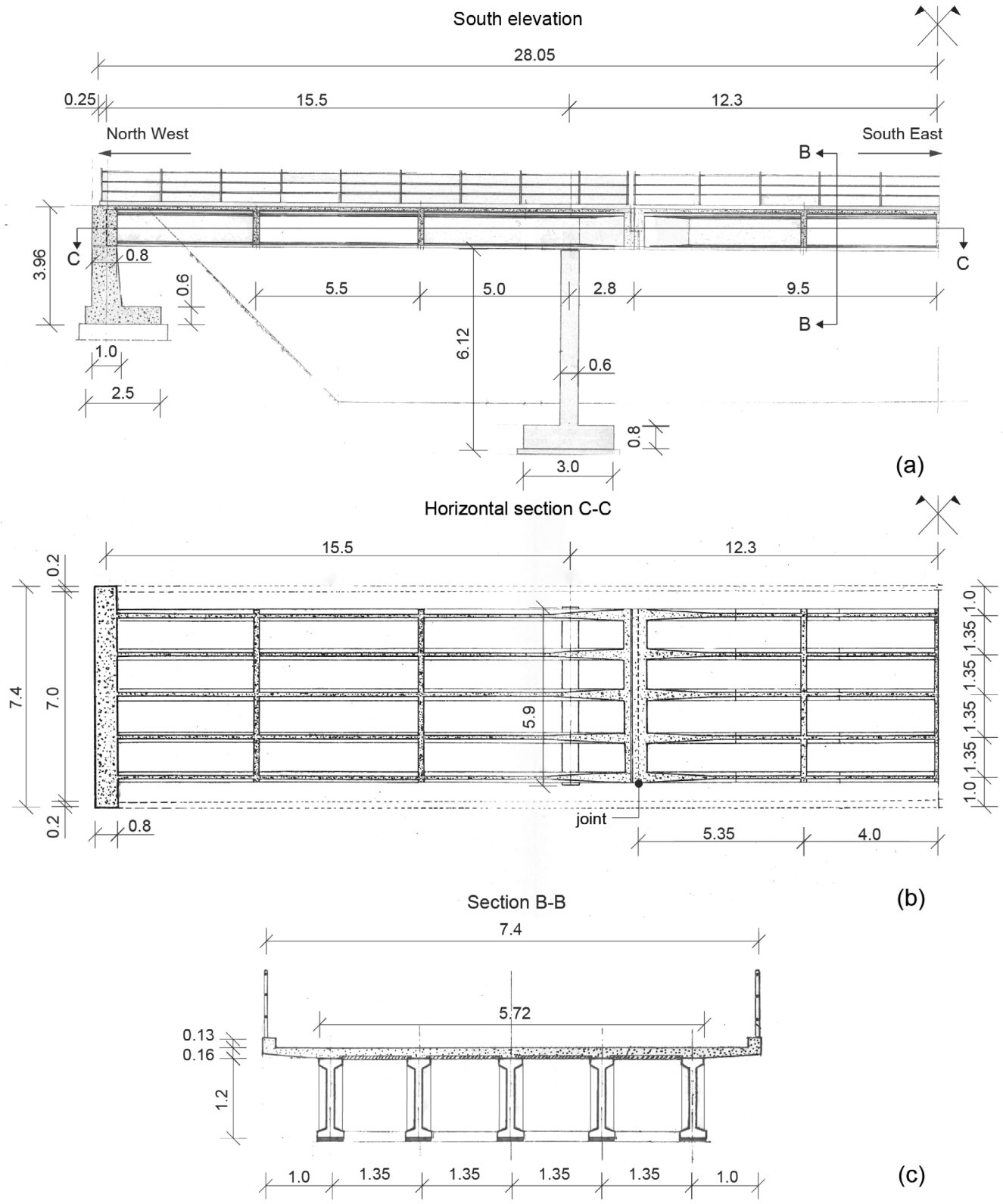

FIGURE 1 Design drawings of the bridge: (a) side view, (b) horizontal section, and (c) vertical cross-section (units: m; adapted from di Prisco et al.[39]).

defects, poor-quality materials, and operational errors. A combination of these issues was responsible for the collapse of the Annone viaduct. In notional damage scenario approaches, assuming the removal of a half-joint while the rest of the bridge remains intact is a practical simplification adopted during the design phase.

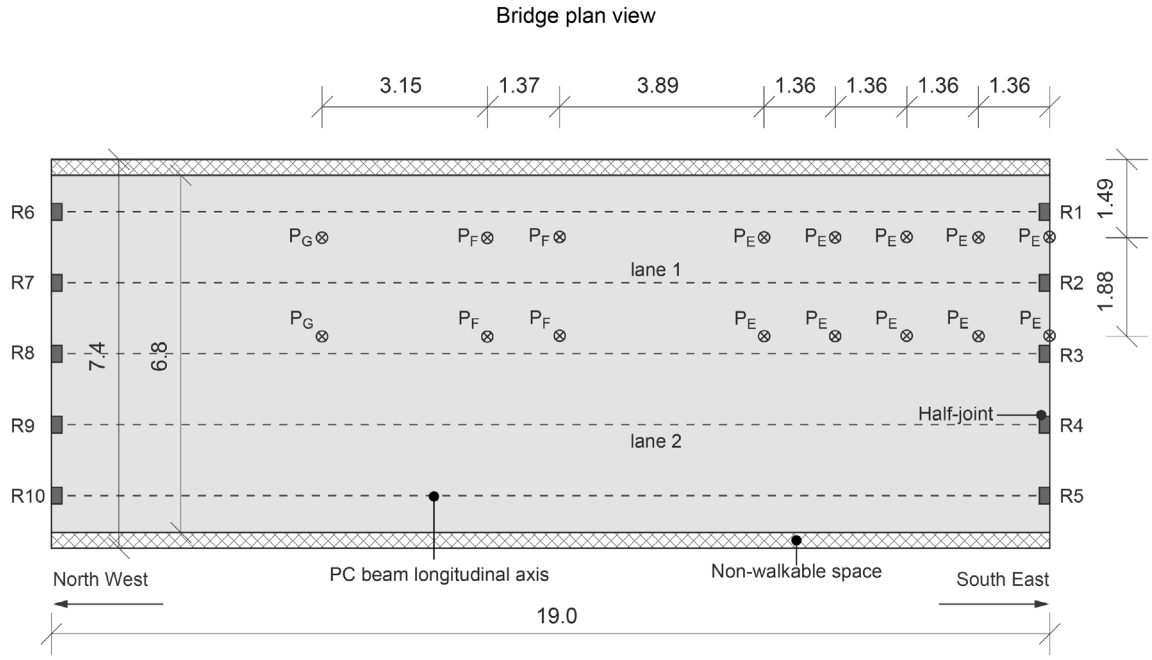

FIGURE 2 Loads on the bridge's central span according to 8-axle heavy truck ($P_E = 69.651$ kN, $P_F = 67.689$ kN, and $P_G = 44.145$ kN; units: m; adapted from Martinelli et al.[38]).

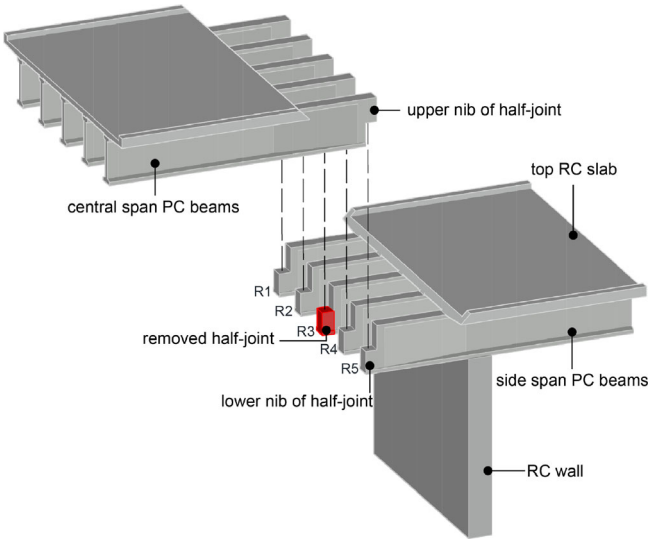

FIGURE 3 Schematic representation of one generic half-joint loss scenario. Reprinted from Martinelli and Colombo.[38]

For each notional removal scenario, a nonlinear FE analysis is carried out by gradually increasing the load multiplier α, in order to evaluate the global response of the structure under increasing load. The details of the model are provided in Section 5. In this study, the ultimate load multiplier α_u is defined for each notional removal scenario as the value of α at the final analysis step before termination due to lack of convergence. It is important to emphasize that the numerical analyses presented here are not intended to determine the bridge ultimate bearing capacity. Instead, due to the notional removal approach, the simulations begin from an already damaged state (i.e., with a removed support) and are limited to evaluating the residual capacity resulting from internal force redistribution.

5 | FINITE ELEMENT MODELS

The numerical models of the Annone overpass are created and analyzed using ABAQUS/Standard.[48] The geometric and material characteristics of the FE models are detailed in the following subsections.

5.1 | Geometrical modeling

Robustness quantification is performed using 3D nonlinear FE models, focusing on the central span of the bridge while excluding the side spans. Geometric parameters are derived from the original design report and structural drawings. A multi-scale approach is adopted for the FE model: the central span, which consists of longitudinal and transverse beams as well as the RC slab, is modeled using shell elements, while the supports of the central span, namely the Gerber saddles of the side spans, are represented by nonlinear translational springs, as shown in Figure 4 and based on previous studies.[38,39]

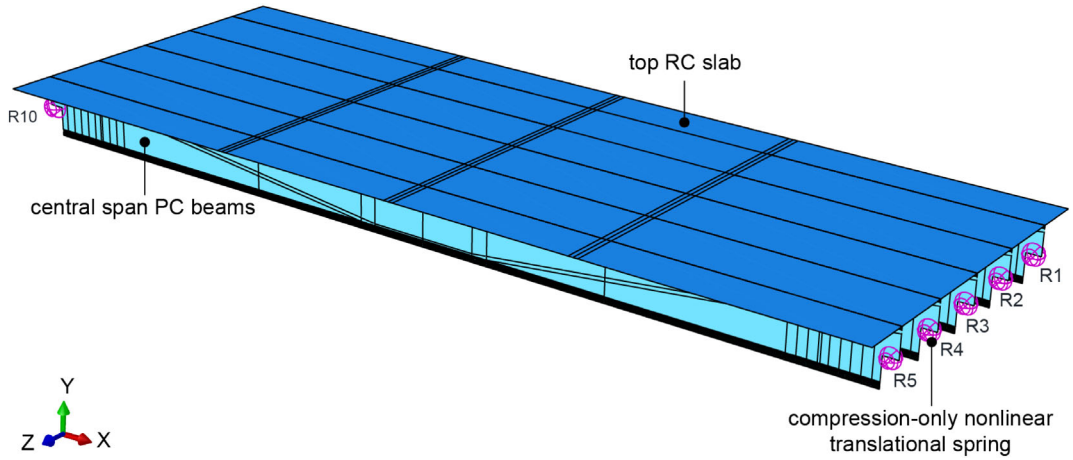

FIGURE 4 Primary structural components and boundary conditions of the FE bridge model.

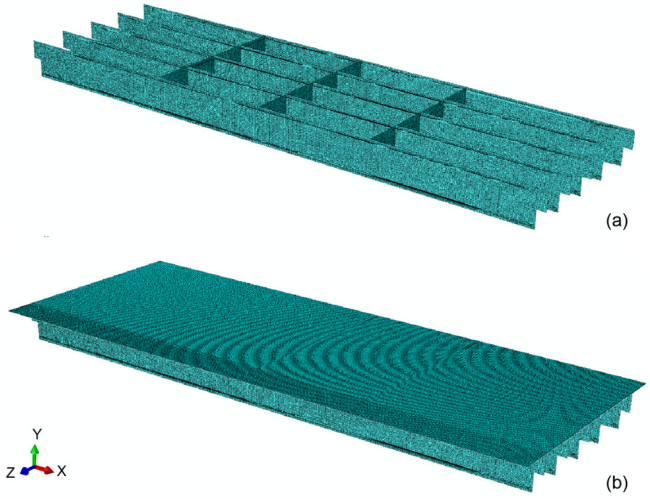

FIGURE 5 3D view of the FE bridge model: (a) central span beam grid and (b) central span deck slab supported by the beam grid.

Figure 5a provides a 3D mesh view of the bridge beam grid, excluding the RC top slab, while Figure 5b illustrates the slab supported by the beam grid. The FE model consists of 412,501 nodes and 163,505 elements, combining different element types to balance computational efficiency and accuracy across regions with varying geometric and mechanical complexity. Specifically, 40,824 linear quadrilateral shell elements of type S4R are used for the bridge deck, while the beam grid is discretized with 121,483 quadratic quadrilateral shell elements of type S8R5 and 1198 quadratic triangular shell elements of type STRI65. S4R elements are four-node linear shell elements with reduced integration and six degrees of freedom (DOF) per node. They are well suited for modeling large, relatively flat regions such as the deck, where stress gradients are moderate, offering a good compromise between accuracy and computational cost. The beam grid—comprising longitudinal PC beams and transverse RC beams—features more complex geometry, stress concentrations, and discontinuities. Therefore, it is modeled using S8R5 and STRI65 elements, which are eight-node and six-node quadratic shell elements, respectively, both with five DOF per node (three translational and two in-plane rotational components). These elements provide improved displacement and stress interpolation, essential for capturing local flexural and shear behavior. A finer mesh size of 40 mm is applied to the beam grid to better resolve local effects, while a coarser 60 mm mesh is used for the deck.

To ensure structural continuity, all components are assembled assuming a perfect bond at the bridge joints, including those between the RC slab and the PC beams, the PC beams and the transverse RC beams, and the RC slab and the transverse RC beams. This assumption reflects the construction method of the overpass.

The concrete components of the bridge are modeled using shell elements, with cross-sections subdivided into layers. Each layer is assigned variable widths based on the cross-sectional properties of the corresponding member. The reinforcement in RC members is represented by equivalent rebar layers, accounting for both transverse and longitudinal reinforcement. This approach ensures that the steel sectional area and effective rebar depth accurately capture the structural behavior of each element. Additionally, a perfect bond is assumed between concrete and steel reinforcement to reflect the composite action of the materials.

A clear distinction must be made between the supporting and supported Gerber saddles, as the construction details of these discontinuity regions (D-regions) can differ significantly. The supporting saddle, located in the lower part of the joint, is generally more exposed to water

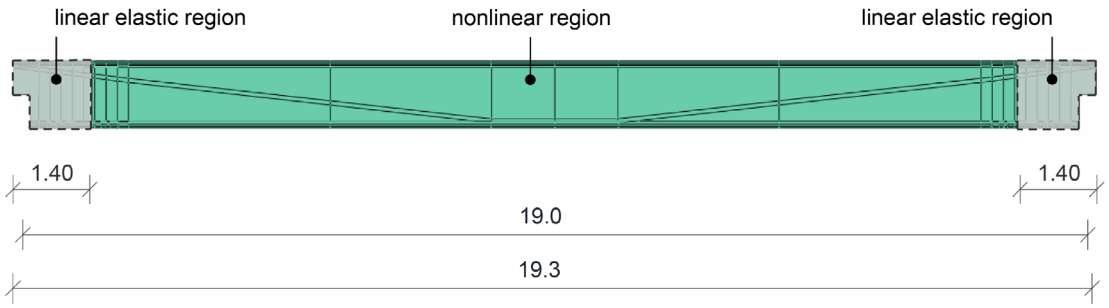

FIGURE 6 Side view of the PC beam with indications of linear and nonlinear material assignment (units: m).

and de-icing salt ingress through the joint from above, making it more susceptible to degradation. In the case under investigation, the supporting saddle was found to be under-reinforced and structurally inadequate, whereas the supported saddle exhibited a more appropriate reinforcement layout. Photographic evidence taken a few hours prior to the collapse (see Figure 7 in di Prisco et al.[39]) shows clear signs of deterioration in the external supporting saddle R1—most notably a shear crack—while the supported saddle showed no visible signs of damage. Accordingly, the supporting saddle is modeled macroscopically and phenomenologically as a nonlinear spring (Section 5.3), whereas the D-region of the supported saddle is assumed to behave in a linear-elastic manner (Figure 6), also to mitigate convergence issues in the end zones of the beams where the prestressing cables terminate.

TABLE 1 Basic concrete material properties (E_c: Young's modulus; ν_c: Poisson's ratio; ρ: density) and plasticity parameters of the CDP model (ψ: dilation angle; ϵ: flow potential eccentricity; f_{b0}/f_{c0}: ratio of biaxial to uniaxial compressive strength; K: Drucker–Prager surface modifier; ξ: viscosity parameter).

Parameter	Value
E_c (MPa)	31,476 (C25)–34,077 (C35)
ν_c (−)	0.2
ρ (kg/m^3)	2400
ψ (°)	13
ϵ (−)	0.1
f_{b0}/f_{c0} (−)	1.16
K (−)	0.7
ξ (−)	1×10^{-4}

5.2 | Material modeling

5.2.1 | Concrete

The structural elements vary in material composition, including different concrete classes and steel grades. Their mechanical properties are defined according to *fib* Model Code 2010[49] and EN 1992-1-1[50] for normal-weight ordinary concrete and high-strength steel reinforcement. The slab and transverse beams are cast-in-situ elements made of C25 concrete, while the longitudinal PC beams utilize C35 concrete, as determined by the experimental campaign conducted by di Prisco et al.[39]

The elastic properties of C25 and C35 concrete, derived from the *fib* Model Code 2010,[49] are listed in Table 1. The inelastic behavior is modeled using the Concrete Damaged Plasticity (CDP) model.[51,52] Since damage effects are not considered in the numerical analyses, the CDP model is applied as an elasto-plastic constitutive law with a non-associated flow rule. The selected plasticity parameters, detailed in Table 1, are based on values from the literature,[53] with a thorough justification provided therein. To enhance numerical stability without significantly altering the mechanical response, a visco-plastic regularization of the constitutive equations is implemented. An increased value of the viscosity parameter ξ—compared to that reported in Table 1—was adopted for the analysis involving the removal of half-joint R1 (i.e., $\xi = 1 \times 10^{-3}$).

In accidental design scenarios, such as those triggered by unforeseen events—modeled in this study through half-joint loss scenarios—characteristic strength values are used. These values, listed in Table 2, define the compressive and tensile constitutive laws of concrete. The uniaxial compressive stress–strain relationship for both C25 and C35 concrete classes follows the nonlinear curve proposed by the *fib* Model Code 2010.[49] Table 2 reports the cylindrical compressive strength f_{ck}, the strain at peak stress ε_{c1}, and the plasticity parameter k.

For uniaxial tension, the mixed stress–strain and stress-crack opening relationship consists of a pre-peak linear segment followed by a post-peak bilinear descending branch. The tensile strength f_{ct} is determined

TABLE 2 Additional concrete material parameters: cylindrical characteristic compressive strength (f_{ck}), strain at maximum compressive stress (ε_{c1}), ultimate strain of concrete in compression ($\varepsilon_{c,lim}$), plasticity number (k), and tensile strength (f_{ct}).

	Compression				Tension
Concrete grade	f_{ck} (MPa)	ε_{c1} (‰)	$\varepsilon_{c,lim}$ (‰)	k (−)	f_{ct} (MPa)
C25	25	2.2	3.5	2.15	2.6
C35	35	2.3	3.5	1.92	3.2

according to the *fib* Model Code 2010,[49] with the necessary mechanical parameters detailed in Table 2. To mitigate mesh dependency, an automatic pseudo-regularization is applied in tension, based solely on mode I fracture energy.

5.2.2 | Steel

In the numerical analyses, an elasto-J2 plastic material model is assumed for both steel rebars and prestressing tendons. The normal steel reinforcement used in the cast-in-situ elements consists of FeB 44 k, with a characteristic yield stress (f_{yk}) of 431 MPa, derived from the reported value of 4400 kg/cm^2 in di Prisco et al.[39] Based on the typical properties of this steel grade, the ultimate tensile strength is assumed to be 540 MPa. Following the *fib* Model Code 2010,[49] a bi-linear stress–strain curve with hardening is adopted for normal reinforcement steel. For the prestressing steel used in the precast PC beams, a characteristic 0.1% proof strength ($f_{p0.1k}$) of 1600 MPa and an ultimate strength (f_{ptk}) of 1765 MPa are assumed. In accordance with the *fib* Model Code 2010,[49] an idealized bi-linear strain–stress curve with hardening is adopted. The elastic and inelastic material parameters for both steel rebars and prestressing tendons used in the numerical analyses are summarized in Table 3.

The pre-stress action on the tendons embedded in the precast beams is modeled by applying equivalent external loads, as detailed by Toniolo and di Prisco.[54] A prestressing stress of $\sigma_p = 981$ MPa is assigned to the three tendon groups in the PC beams.

5.3 | Half-joint idealization

Previous studies[38,39] have modeled the connection between the mid-span of the bridge and the side spans using uniaxial, compression-only nonlinear translational springs at each half-joint. These springs, arranged in two sets of five on either side of the mid-span (R1–R10 in Figure 2), exhibit a multilinear load–displacement (P–δ) response influenced by cracking patterns and rigid body motion. The nonlinear behavior follows the approach detailed in di Prisco et al.,[39] with key principles summarized below.

TABLE 3 Elastic and inelastic steel material parameters: modulus of elasticity of reinforcing steel (E_s), modulus of elasticity of prestressing steel (E_p), Poisson coefficient (ν_s), density (ρ), characteristic yield strength of reinforcing steel (f_{yk}), tensile strength of reinforcing steel (f_{tk}), characteristic 0.1% proof strength of prestressing steel ($f_{p0.1k}$), characteristic strength of prestressing steel (f_{ptk}), characteristic strain at maximum force of reinforcing steel (ε_{uk}), characteristic strain at maximum force of prestressing steel (ε_{puk}).

Parameter	Value for steel rebar	Value for prestressing tendon
E_s (MPa)	200,000	-
E_p (MPa)	-	195,000
ν_s (−)	0.3	0.3
ρ (kg/m^3)	7850	7850
f_{yk} (MPa)	431	-
f_{tk} (MPa)	540	-
$f_{p0.1k}$ (MPa)	-	1600
f_{ptk} (MPa)	-	1765
ε_{uk} (%)	7.5	-
ε_{puk} (%)	-	3.5

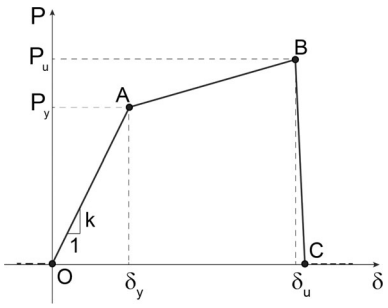

FIGURE 7 Simplified nonlinear behavior for intact half-joints.

The total displacement (δ) consists of two components: the elastic deflection of the side-span PC beam and the rigid body motion caused by cracking at the half-joint. Half-joints that are not damaged are assumed to have reinforcement without corrosion. The P–δ relationship is defined by three critical parameters: the yielding load (P_y), the ultimate load (P_u), and the ultimate displacement (δ_u), as illustrated in Figure 7. The values of

TABLE 4 Simplified nonlinear behavior for intact half-joints in terms of load vs. displacement (points O, A, B, and C indicated in Figure 7).

Point	Displacement δ (m)	Load P (N)
O	0.000	0
A	5.886×10^{-3}	356,700
B	55.676×10^{-3}	578,500
C	57.000×10^{-3}	0

P_y and P_u are obtained using strut-and-tie models (cases C and D) from di Prisco et al.,[39] while δ_u is determined from the ultimate crack opening (w_u), calculated based on *fib* Model Code 2010[49] and *fib* Bulletin 63.[55] A detailed derivation of w_u is available in di Prisco et al.[39] Once P_u is reached, the BC branch eliminates the contribution of the spring. Table 4 summarizes the force-displacement values for intact Gerber saddles.

6 | RESULTS AND DISCUSSION

The FE model described in Section 5 enabled the assessment of ρ_s, ρ_Φ, and R_3, as defined in Equations 1 to 3. Figure 8 presents the reaction forces in half-joints R1 to R5, comparing the intact structure with various half-joint loss scenarios outlined in Section 4. A horizontal dashed line indicates the ultimate capacity of the half-joint (see Section 5.3). As expected, a removed half-joint carries no reaction force. Half-joint reactions are reported for a unit load multiplier value unless the ultimate load multiplier was lower than 1 ($\alpha_u < 1$). Removal of the end-loaded half-joint R1 results in a strong load eccentricity that causes unloading of the opposite half-joint R5 (Figure 8).

To provide a comprehensive understanding of the bridge overall behavior, Figure 9 depicts the load multiplier α versus the midspan vertical displacement of the central PC beam for each support-removal scenario, as well as for the intact condition. The ultimate load multiplier α_u for each scenario is indicated in Figure 9 next to the corresponding curve. While Martinelli et al.[38] reported an ultimate load multiplier of $\alpha_u = 0.89$ for the removal of half-joint R1, the present FE model predicts a lower value of $\alpha_u = 0.50$. This difference indicates that accounting for material nonlinearities not only in the half-joints but throughout the entire structure allows for consideration of structural ultimate conditions that may arise not solely from half-joint failure. In the case of end half-joint R1 removal, the analysis terminates before the adjacent half-joint R2 reaches its ultimate capacity—marking a departure from the behavior observed in the simplified model.[38] This outcome is attributed to

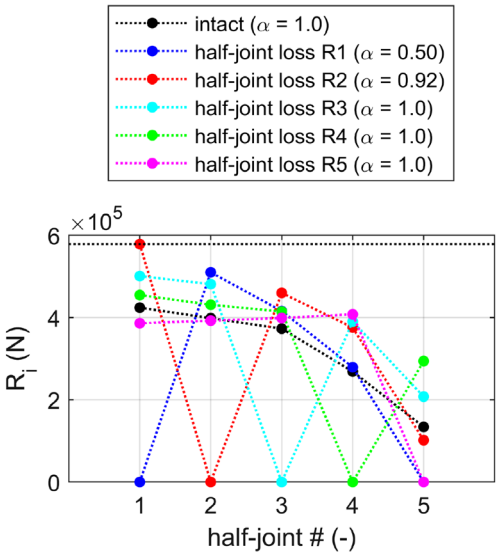

FIGURE 8 Reactions in half-joints R1–R5 for various half-joint loss scenarios, including the intact situation.

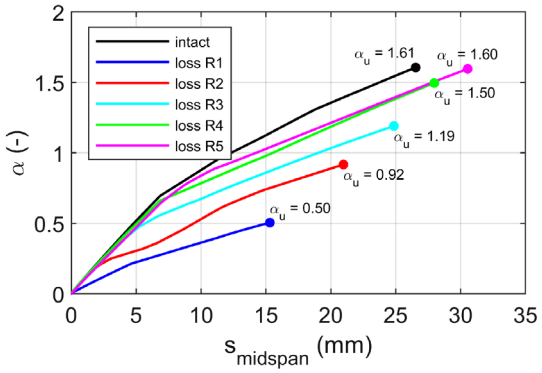

FIGURE 9 Load multiplier α vs. midspan displacement $s_{midspan}$ for different half-joint loss scenarios.

the bearing capacity of the top RC slab, characterized by transverse unit moments that are very close to its maximum capacity over half-joint R2 (see Figure 10b).

Next, the reaction forces in half-joints R1 to R5 following the loss of half-joint R2 are shown in Figure 8. These forces reveal that the adjacent half-joint R1 reaches its ultimate bearing capacity ($F_{k,ult}$). However, numerical convergence issues arise before the structure can support the full 8-axle truck load, with the load multiplier α remaining below 1 ($\alpha_u = 0.92$). The premature termination of these analyses underscores the crucial role of the end-loaded half-joint R1—and, to a lesser extent, R2—in structural load distribution.

Load multiplier (α) versus midspan deflection curves for the remaining saddle removal cases (R3, R4, and R5) are shown in Figure 9, revealing a progressively increasing ultimate load multiplier of 1.19, 1.50, and 1.60.

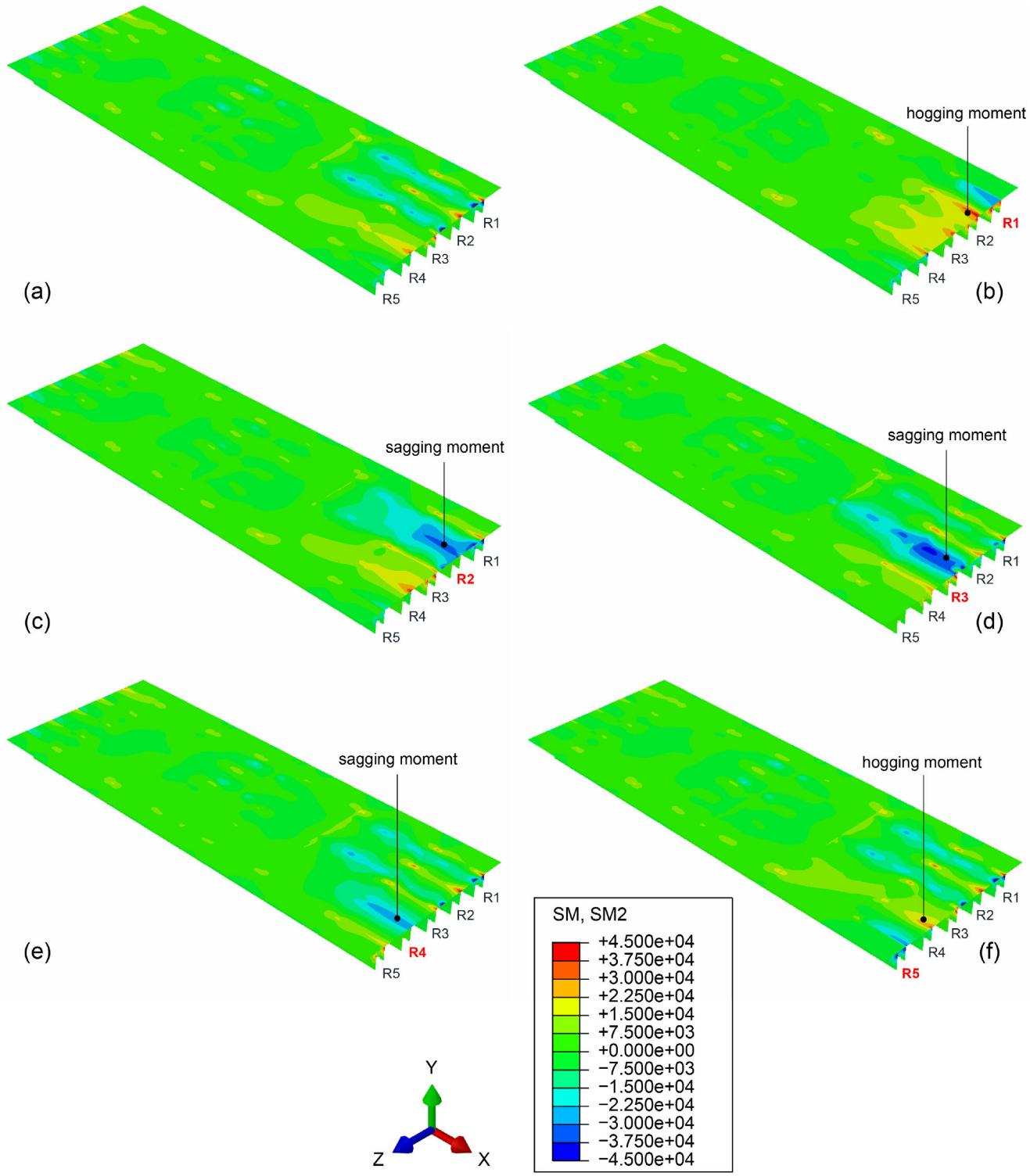

FIGURE 10 Transverse bending moment per unit length (SM2) at the end of the analysis for (a) the intact scenario and (b–f) half-joint loss scenarios R1–R5 (units: Nm; removed half-joint shown in bold red).

Additionally, Figure 10 illustrates the transverse bending moment (labeled as SM2 in the figure) at the end of the analysis for both the intact scenario and the half-joint loss scenarios (R1–R5), with the removed half-joints shown in bold red. This figure highlights the crucial role of the top slab in redistributing loads following the removal of a Gerber saddle.

In the cases of the intact half-joint, removal of half-joint R2, and removal of half-joint R4, the ultimate load multiplier (α_u) is reached when the end-loaded half-joint

R1 attains its maximum load-bearing capacity. In the case of removing the central half-joint R3, the assumed ultimate condition is governed by transverse bending failure (sagging moment) of the top slab between Gerber half-joints R2 and R4 (Figure 10d). In the case of removing the end half-joint R5 (the farthest from the load), the α_u value corresponds to transverse bending failure (hogging moment) in the slab above half-joint R4 (Figure 10f). In this latter case, the distribution of moments in the transverse direction of the top slab is very similar to the intact situation (compare Figure 10a,f), which also explains the very similar ultimate load multipliers.

Due to the premature loss of numerical convergence before reaching the full truck load ($\alpha = 1$), particularly in the R1 half-joint removal scenario, robustness is evaluated based on the lowest load level observed in the numerical analyses. This approach ensures a consistent comparison across all half-joint removal cases. Figures 11 and 12 present displacement- and energy-based indicators at 50% of the truck load ($\alpha = 0.5$), which corresponds in intensity to the design-phase load applied to a single lane.[43]

The index ρ_s, calculated using Equation (1), is based on the midspan vertical displacement of the central PC beam, considered representative of the overall bridge behavior. For the purpose of evaluating robustness indicators, the choice between adopting the midspan displacement of the central beam or the outer beams has a negligible influence. In contrast, using the displacement at the half-joint may lead to lower values of the robustness indicator ρ_s, as shown in Martinelli et al.[38]; however, this latter choice is not representative of the global behavior of the bridge. The results align with the general trend observed in Martinelli et al.[38] using a simplified nonlinear FE model. However, the robustness indicators in this study are lower due to the inclusion of nonlinear material properties, which enhance energy dissipation

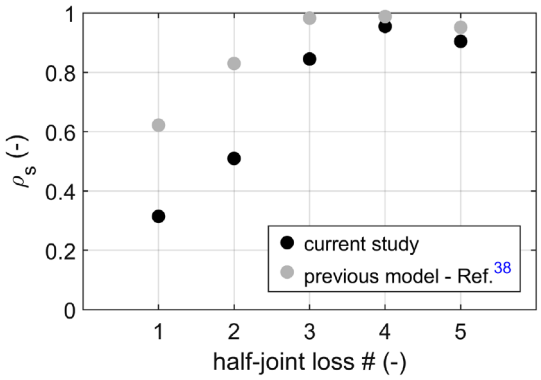

FIGURE 11 Robustness index ρ_s for different half-joint loss scenarios.

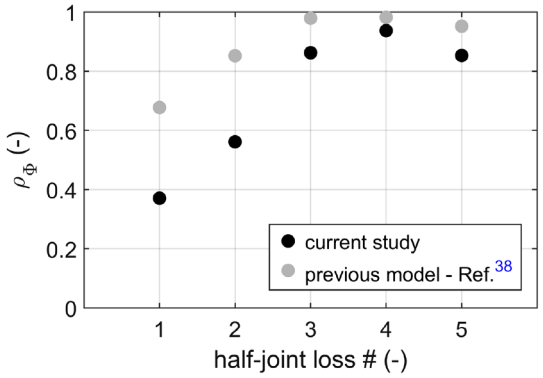

FIGURE 12 Robustness index ρ_Φ for different half-joint loss scenarios.

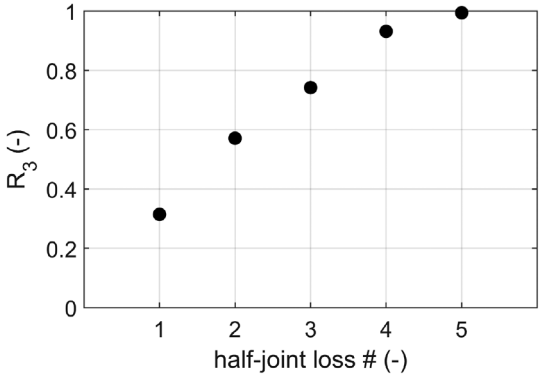

FIGURE 13 Robustness index R_3 for different half-joint loss scenarios.

and allow for greater displacements, resulting in a more flexible structural response. As expected, the removal of the end half-joint R1 in the loaded lane represents the most unfavorable condition. Figures 11 and 12 show similar values and trends for the ρ_s and ρ_Φ indicators, converging toward conditions of lower robustness and increased susceptibility to progressive collapse.

The evaluation of the robustness indicator R_3 requires determining the bridge ultimate load capacity under various support-loss scenarios, including the intact condition. After reaching $\alpha = 1$ for both the intact model and the cases involving the removal of half-joints R3, R4 and R5, the load is further increased to identify the maximum load-bearing capacity in each configuration. These values are then used in Equation (3) to compute R_3. Figure 13 presents the robustness index R_3, largely confirming the trends observed in Figures 11 and 12, particularly regarding the most critical scenario.

It is important to note that, in this study, the ultimate bearing capacity—required for the calculation of R_3—corresponds to the final analysis step before termination due to non-convergence. In finite element models,

failure to converge does not necessarily indicate the attainment of an ultimate limit state (let alone the collapse load of the structure); rather, it may be associated with local instabilities. In the present case, the ultimate load multiplier, α_u, is either associated with the attainment of the ultimate capacity in a half-joint (in the cases of the intact scenario, and the loss of half-joints R2 and R4), or with a value very close to this capacity, but accompanied by failure of the top slab due to transverse bending (in the cases of the loss of half-joints R1, R3, and R5).

Consistent with the findings of Martinelli et al.[38] using a simplified nonlinear model, reaching the load-bearing capacity in a second half-joint invariably results in the loss of numerical convergence, likely leading to structural collapse. The ultimate capacity when half-joint R5 is removed is comparable to that of the intact structure (Figure 9). This result is due to efficient load redistribution, where the remaining supports share the load almost uniformly, which explains the R_3 value close to one in Figure 13.

7 | CONCLUSIONS

This study investigates the structural robustness of reinforced concrete (RC) girder bridges with half-joints, using the Annone viaduct as a case study. The overpass, a precast concrete structure built in the 1960s, features three spans, two joints, and five Gerber saddles per joint. It collapses catastrophically in 2016 following the passage of a heavy truck. Robustness is assessed using a notional removal approach, where the removal of each individual half-joint is analyzed separately to assess its impact on the overall structural response. A nonlinear finite element (FE) model is developed, including full material nonlinearities to better capture both global and local failure mechanisms. Three deterministic robustness indicators are employed—displacement-based (ρ_s), energy-based (ρ_Φ), and capacity-based (R_3)—adapting approaches traditionally developed for buildings to the context of RC bridges with Gerber saddles.

This research corroborates the findings of previous studies,[38] confirming that in the case of the half-joint RC girder bridge under investigation—featuring a rigid deck integrated with longitudinal and transverse beams—the primary resistance mechanism following the loss of a half-joint relies on the flexural-transverse and torsional stiffness of the beam grid and top slab, enabling effective load redistribution to adjacent half-joints. Additionally, the five Gerber saddles at each joint of the central suspended span play a crucial role in this redistribution process. While the failure of a single Gerber saddle does not necessarily lead to overall collapse, the ultimate failure of a second Gerber saddle inevitably triggers the collapse of the entire central span.

The results demonstrate the critical role of half-joint R1, located at the extremity of the loaded lane, in maintaining structural stability. Its removal results in the most severe structural response, characterized by a high transverse moment in the top slab near the adjacent half-joint R2 and a significant redistribution of internal forces. In contrast, the removal of other half-joints has a lesser impact on overall bridge stability, with load multipliers increasing gradually as Gerber saddles are removed progressively farther from the loaded lane. These findings highlight the high sensitivity of half-joint bridges to local failures and underscore the importance of early detection and maintenance of these critical components.

In all removal scenarios, the three robustness indicators yield consistent trends, though their absolute values are lower than those reported in prior studies using simplified models. This suggests that modeling material nonlinearities leads to more conservative (and possibly more realistic) estimates of structural robustness.

Although the findings are based on a single case study, the methodology illustrates how robustness indicators can be meaningfully applied to half-joint bridges. The results support the idea that traditional robustness estimates—based on linear elastic models or other simplified approaches—may overpredict the reserve capacity of half-joint bridges, potentially underestimating their vulnerability to progressive collapse.

Care must be taken when using robustness indicators based on ultimate capacity, particularly when calculated using finite element models, as local instabilities may lead to premature numerical convergence failure, which does not necessarily reflect the true ultimate bearing capacity of the bridge.

From a practical perspective, this study underscores the urgent need for proactive maintenance strategies for aging half-joint bridges. Regular inspections, early detection of corrosion and cracking, and targeted strengthening interventions significantly enhance their robustness. Furthermore, the findings suggest that current design guidelines for robustness assessment should be refined to better account for the influence of nonlinear behavior on structural performance.

ACKNOWLEDGMENTS

The contribution of Pedro Jose Verbel Arroyo, who developed the numerical model of the bridge as part of his MSc thesis in Civil Engineering at Politecnico di Milano, is gratefully acknowledged. Open access publishing facilitated by Politecnico di Milano, as part of the Wiley - CRUI-CARE agreement.

CONFLICT OF INTEREST STATEMENT

The authors declare no conflicts of interest.

DATA AVAILABILITY STATEMENT

The data that support the findings of this study are available from the corresponding author upon reasonable request.

ORCID

Paolo Martinelli https://orcid.org/0000-0003-1029-7744
Matteo Colombo https://orcid.org/0000-0001-6457-7894

REFERENCES

1. Starossek U. Typology of progressive collapse. Progressive collapse of structures. London, UK: ICE Publishing; 2017. p. 18–42. https://doi.org/10.1680/pcos.61682.018
2. Derseh SA, Mohammed TA. Bridge structures under progressive collapse: a comprehensive state-of-the-art review. Results Eng. 2023;18:101090. https://doi.org/10.1016/j.rineng.2023.101090
3. Wisniewski D, Casas JR, Ghosn M. Load capacity evaluation of existing railway bridges based on robustness quantification. Struct Eng Int. 2006;16:161–6. https://doi.org/10.2749/101686606777962440
4. Ghosn M, Moses F, Frangopol DM. Redundancy and robustness of highway bridge superstructures and substructures. Struct Infrastruct Eng. 2010;6:257–78. https://doi.org/10.1080/15732470802664498
5. Jiang R, Wu Q, Chen Y, Yi X, Tu J. About the structural robustness of through arch bridges. Appl Mech Mater. 2012;178:2412–7. https://doi.org/10.4028/www.scientific.net/AMM.178-181.2412
6. Wang M, Zhou Z. Progressive collapse and structural robustness of bridges. Appl Mech Mater. 2012;193:1021–4. https://doi.org/10.4028/www.scientific.net/AMM.193-194.1021
7. Olmati P, Brando F, Gkoumas K. Robustness assessment of a steel truss bridge. Proceedings of the 2013 structural congress. Reston: American Society of Civil Engineers (ASCE); 2013. p. 250–61. https://doi.org/10.1061/9780784412848.023
8. Anitori G, Casas JR, Ghosn M. Redundancy and robustness in the design and evaluation of bridges: European and North American perspectives. J Bridge Eng. 2013;18:1241–51. https://doi.org/10.1061/(ASCE)BE.1943-5592.0000545
9. Cavaco ES, Casas JR, Neves LAC, Huespe AE. Robustness of corroded reinforced concrete structures—a structural performance approach. Struct Infrastruct Eng. 2013;9:42–58. https://doi.org/10.1080/15732479.2010.515597
10. Au FTK, Leung CCY, Kwan AKH. Collapse mechanism and robustness of precast segmental bridges. Proc Institut Civil Eng Bridge Eng. 2014;167:303–14. https://doi.org/10.1680/bren.11.00045
11. Cavaco ES, Neves LAC, Casas JR. On the robustness to corrosion in the life cycle assessment of an existing reinforced concrete bridge. Struct Infrastruct Eng. 2018;14:137–50. https://doi.org/10.1080/15732479.2017.1333128
12. Shoghijavan M, Starossek U. Structural robustness of long-span cable-supported bridges in a cable-loss scenario. J Bridge Eng. 2018;23:04017133. https://doi.org/10.1061/(ASCE)BE.1943-5592.0001186
13. Bontempi F. Elementary concepts of structural robustness of bridges and viaducts. J Civil Struct Health Monit. 2019;9:703–17. https://doi.org/10.1007/s13349-019-00362-7
14. Fan BH, Su JZ, Chen BC. Condition evaluation for through and half-through arch bridges considering robustness of suspended deck systems. Adv Struct Eng. 2021;24:962–76. https://doi.org/10.1177/1369433220945835
15. Shoghijavan M, Starossek U. Developing a robustness index for parallel load-bearing systems. Eng Struct. 2021;244:112742. https://doi.org/10.1016/j.engstruct.2021.112742
16. Buitrago M, Bertolesi E, Calderón PA, Adam JM. Robustness of steel truss bridges: laboratory testing of a full-scale 21-metre bridge span. Structures. 2021;29:691–700. https://doi.org/10.1016/j.istruc.2020.12.005
17. Saracco U, Felitti M, Oliveto F, Alvaro MR, Formisano A. Robustness evaluation of a steel bridge in the district of Potenza (Italy). Procedia Struct Integr. 2023;44:721–8. https://doi.org/10.1016/j.prostr.2023.01.094
18. Caredda G, Porcu MC, Buitrago M, Bertolesi E, Adam JM. Analysing local failure scenarios to assess the robustness of steel truss-type bridges. Eng Struct. 2022;262:114341. https://doi.org/10.1016/j.engstruct.2022.114341
19. Acharya P, Hao R, Lin W, He J. Assessing structural robustness of composite I-girder bridges through a work-based approach and nonlinear numerical analyses. Struct Infrastruct Eng. 2024;1–20. https://doi.org/10.1080/15732479.2024.2435913
20. Dhir PK, Losanno D, Tubaldi E, Parisi F. Performance and robustness assessment of roadway masonry arch bridges to scour-induced damage using multiple traffic load models. Eng Struct. 2025;325:119441. https://doi.org/10.1016/j.engstruct.2024.119441
21. CNR. CNR DT 214/2018, guide to design of structures for robustness. Rome, Italy: Consiglio Nazionale delle Ricerche (CNR); 2021.
22. André J, Anghileri M, Belletti B, Biondini F, Caspeele R, Demonceau JF, et al. Guidance on the design for structural robustness. Luxembourg: Publications Office of the European Union; 2024. https://doi.org/10.2760/525706
23. Moreira V, Fernandes J, Matos J, Olivera D. Robustness as performance indicator for masonry arch bridges. COST Action TU1406 Eb. 1st Workshop Meeting. Geneva: ETH-Zürich; 2016.
24. Biondini F, Frangopol D. Life-cycle robustness of deteriorating concrete structures. International conference on performance-based life-cycle structural engineering, Brisbane, QLD, Australia. Brisbane, Australia: University of Queensland; 2015.
25. Björnsson I, Thelandersson S. Robustness analysis of bridges when exposed to train collision due to derailment. COST ACTION C26 urban habitat construction catastrophic events. Boca Raton, FL: CRC Press (Taylor & Francis Group); 2010. p. 603–8.
26. Galano S, Losanno D, Pecce MR. Prestressed reinforced concrete bridges: state of art of the Italian existing stock. Proceedings of the Italian concrete conference. Napoli, Italy; 12–15 October 2022. Erba, Italy: GWMAX; 2022.
27. Autostrade per l'Italia. *Report di analisi delle principali tipologie strutturali di opere presenti sulla rete ASPI*. (In Italian). 2022.

28. Ministero delle Infrastrutture e della Mobilità Sostenibile (MIMS). *Linee guida per la classificazione e gestione del rischio, la valutazione della sicurezza ed il monitoraggio dei ponti esistenti*. (In Italian). 2022.
29. Mattock AH, Chan TC. Design and behavior of dapped-end beams. PCI J. 1979;24(6):28–45. https://doi.org/10.15554/pcij.11011979.28.45
30. Hamoudi AA, Phang MKS, Bierweiler RA. Diagonal shear in prestressed concrete dapped-beams. J Am Concr Inst. 1975;72(7):347–50. https://doi.org/10.14359/11140
31. Desnerck P, Lees JM, Morley CT. Impact of the reinforcement layout on the load capacity of reinforced concrete half-joints. Eng Struct. 2016;127:227–39. https://doi.org/10.1016/j.engstruct.2016.08.061
32. Mata-Falcón J, Pallarés L, Miguel PF. Proposal and experimental validation of simplified strut-and-tie models on dapped-end beams. Eng Struct. 2019;183:594–609. https://doi.org/10.1016/j.engstruct.2019.01.010
33. Flores Ferreira K, Rampini MC, Zani G, Colombo M, di Prisco M. Experimental investigation on the use of fabric-reinforced cementitious mortars for the retrofitting of reinforced concrete dapped-end beams. Struct Concr. 2023;24(4):4577–605. https://doi.org/10.1002/suco.202200743
34. Don W, Suryanto B, Tambusay A, Suprobo P. Forensic assessments of the influence of reinforcement detailing in reinforced concrete half-joints: a nonlinear finite element study. Structures. 2022;38:689–703. https://doi.org/10.1016/j.istruc.2022.02.029
35. Spinella N, Messina D. Load-bearing capacity of Gerber saddles in existing bridge girders by different levels of numerical analysis. Struct Concr. 2023;24(1):211–26. https://doi.org/10.1002/suco.202200279
36. De Domenico D, Spinella N, Messina D, Mazzeo M, Recupero A. Structural behavior of deteriorated Gerber half-joints in highway overpasses by nonlinear finite element analysis combined with a simplified uniform-corrosion model. Struct Concr. 2025. https://doi.org/10.1002/suco.202400556
37. Flores Ferreira K, Rampini MC, Belletti B, Calcavecchia B, Camata G, D'Angela D, et al. Reinforced concrete dapped-end beams for existing bridges: reliability of finite element models. Struct Concr. 2025;26:4496–531. https://doi.org/10.1002/suco.202400365
38. Martinelli P, Colombo M, di Prisco M. Robustness assessment of half-joint RC girder bridges. Eng Struct. 2024;306:117712. https://doi.org/10.1016/j.engstruct.2024.117712
39. di Prisco M, Colombo M, Martinelli P. Structural aspects of the collapse of a RC half-joint bridge: case of the Annone overpass. J Bridge Eng. 2023;28:05023007. https://doi.org/10.1061/jbenf2.beeng-6063
40. Adam JM, Parisi F, Sagaseta J, Lu X. Research and practice on progressive collapse and robustness of building structures in the 21st century. Eng Struct. 2018;173:122–49. https://doi.org/10.1016/j.engstruct.2018.06.082
41. Biondini F, Restelli S. Damage propagation and structural robustness. Life-cycle civil engineering—proceedings of the 1st international symposium on life-cycle civil engineering (IALCCE). Boca Raton, FL: CRC Press (Taylor & Francis Group); 2008. p. 131–6. https://doi.org/10.1201/9780203885307.ch14
42. Frangopol DM, Curley J. Effects of damage and redundancy on structural reliability. J Struct Eng. 1987;113(7):1533–49. https://doi.org/10.1061/(ASCE)0733-9445(1987)113:7(1533)
43. Ministero dei Lavori Pubblici. Circular 14 February 1962 No. 384—Norme relative ai carichi per il calcolo dei ponti stradali. Italia: Ministero dei Lavori Pubblici; 1962 (In Italian).
44. Ministero delle Infrastrutture, NTC. Aggiornamento delle norme tecniche per le costruzioni. (In Italian); 2018. Decreto del Ministro delle Infrastrutture del 17 gennaio 2018, Gazzetta Ufficiale Serie Generale n. 42 del 20–02–2018. 2018.
45. Fédération Internationale du Béton (fib). fib model code for concrete structures 2020. Final draft. Lausanne: Fédération Internationale du Béton; 2023.
46. Rodríguez D, Brunesi E, Nascimbene R. Fragility and sensitivity analysis of steel frames with bolted-angle connections under progressive collapse. Eng Struct. 2021;228:111508. https://doi.org/10.1016/j.engstruct.2020.111508
47. Martinelli P, Colombo M, Ravasini S, Belletti B. Application of an analytical method for the design for robustness of RC flat slab buildings. Eng Struct. 2022;258:114117. https://doi.org/10.1016/j.engstruct.2022.114117
48. Dassault Systèmes. Abaqus analysis user's manual—version 2024. Vélizy-Villacoublay, France: Dassault Systèmes Simulia Corp.; 2024.
49. Fédération Internationale du Béton (fib). fib model code for concrete structures 2010. Hoboken: John Wiley & Sons; 2013. https://doi.org/10.1002/9783433604090
50. Eurocode 2: design of concrete structures—part 1-1: general rules and rules for buildings. BS EN 1992-1-1. Brussels: Comité Européen de Normalisation (CEN); 2004.
51. Lubliner J, Oliver J, Oller S, Oñate E. A plastic-damage model for concrete. Int J Solids Struc. 1989;25(3):299–326. https://doi.org/10.1016/0020-7683(89)90050-4
52. Lee J, Fenves GL. Plastic-damage model for cyclic loading of concrete structures. J Eng Mech. 1998;124(8):892–900. https://doi.org/10.1061/(ASCE)0733-9399(1998)124:8(892)
53. Alfarah B, López-Almansa F, Oller S. New methodology for calculating damage variables evolution in plastic damage model for RC structures. Eng Struct. 2017;132:70–86. https://doi.org/10.1016/j.engstruct.2016.11.022
54. Toniolo G, di Prisco M. Prestressed beams. Reinforced concrete design to Eurocode 2. Springer tracts in civil engineering. Cham: Springer; 2017. https://doi.org/10.1007/978-3-319-52033-9_10
55. Fédération Internationale du Béton (fib). fib Bulletin 63: Design of Precast Concrete Structures Against Accidental Actions. Lausanne: Fédération Internationale du Béton (fib); 2012.

AUTHOR BIOGRAPHIES

Paolo Martinelli, Department of Civil and Environmental Engineering, Politecnico di Milano, Milan, Italy. Email: paolo.martinelli@polimi.it.

Matteo Colombo, Department of Civil and Environmental Engineering, Politecnico di Milano, Milan, Italy. Email: matteo.colombo@polimi.it.

How to cite this article: Martinelli P, Colombo M. Impact of half-joint failures on RC girder bridges: A robustness quantification study. Structural Concrete. 2025. https://doi.org/10.1002/suco.70336